GSA DATA REPOSITORY 2013285

Variation of East Asian monsoon precipitation during the past 21 ka and potential CO_2 forcing

Huayu Lu*, Shuangwen Yi, Zhengyu Liu, Joseph A. Mason, Dabang Jiang, Jun Cheng, Thomas Stevens, Zhiwei Xu, Enlou Zhang, Liya Jin, Zhaohui Zhang, Zhengtang Guo, Yi Wang, Bette Otto-Bliesner
*Corresponding author: huayulu@nju.edu.cn

DATA REPOSITORY ITEM DR1

Optically Stimulated Luminescence Dating of the Loess Sediments

1. Sample preparation and laboratory methods

We took samples from three typical loess sections (Yulin (YL), Luochuan (LC) and Xunyi (XY) sections) (Fig. DR1 and Fig. 1) in Chinese Loess Plateau. All of the samples for optically stimulated luminescence (OSL) dating were collected by hammering stainless steel tubes into cleaned vertical sections, sealed with black plastic bags to avoid light exposure and moisture loss. In the laboratory (here refer to YL and LC sections, the OSL ages of XY section has been reported by (Stevens et al., 2006, 2008), see the papers for details.), quartz grains (63-90 μm) were purified using routine laboratory protocols, e.g. sediments at each end of the tube were scraped away and used for dose rate and water content measurement. While the light unexposed material in middle part of the tube were treaded with 10% HCl and 30% H_2O_2 to remove carbonate and organic matter; etched by 40% HF for 40 minutes to remove feldspar grains and re-sieved, checked by the IR-test protocol (Duller, 2003). They were considered pure enough when natural and regenerated signal ratios of the infrared stimulated luminescence (IRSL) to the blue-light stimulated luminescence (BLSL) were less than 10%. If not, the 40 minutes etching in 40% H_2SiF_6 was repeated. The isolated quartz grains were mounted on 10 mm diameter steel discs with silicon oil. Luminescence signals were measured on a Risø TL/OSL-DA-20C/D reader fitted with blue-green diodes ($\lambda = 470 \pm 30$ nm; 40 mW cm^{-2}) and IR- LEDs emitting at 875 nm (Bøtter-Jensen et al., 2003). Luminescence was detected by a 9235QA photomultiplier tube through a 7.5 mm thick U-340 filter.

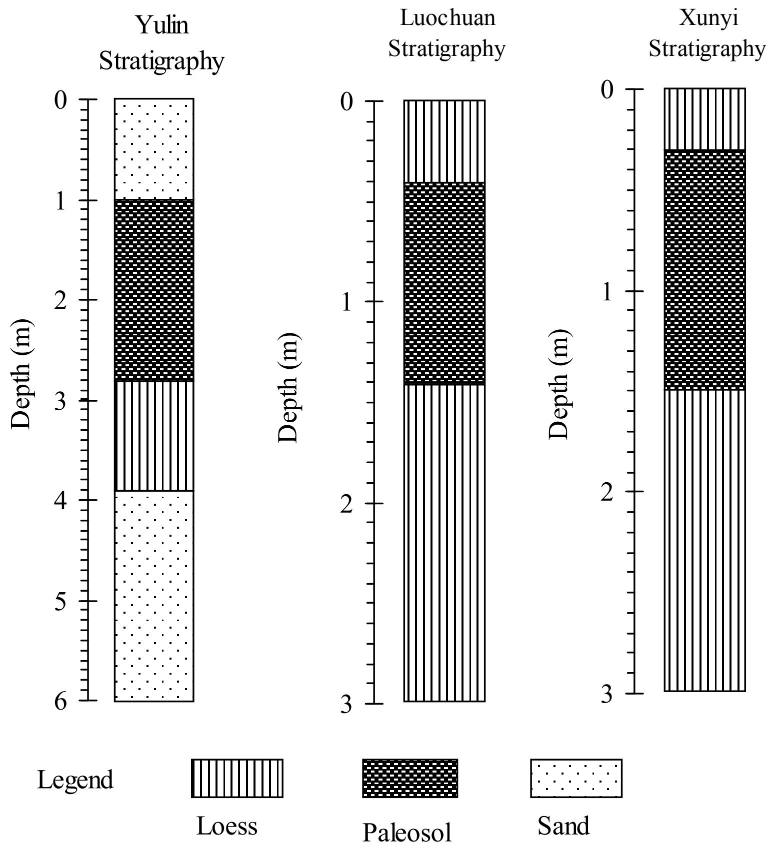

Figure DR1. Pedostraigraphy of the loess-paleosol sections at Yulin, Luochuan and Xunyi.

For estimating dose rate to grains, concentrations of ^{238}U, ^{232}Th and ^{40}K were measured by Neutron Activation Analysis (NAA). Average water content of 15 ± 4% was assumed for samples of LC section (Buylaert et al., 2007) while *in situ* water content (mass of moisture/dry mass (Aitken, 1998)) was used by weighing the sample before and after drying for samples of YL sections. Using the revised dose rate conversion factors of Adamiec et al. (1998) and water content attenuation factors (Aitken, 1998); the elemental concentration was converted into effective dose rate. The calculation was performed using the 'AGE' program of Grün (2009), which include a calculation of the cosmic ray contribution to the dose rate.

A total of 69 samples have been dated with the OSL technique, 36 ages reported for the first time in this paper are in Table DR1 and Table DR2, the other ages have been reported (Stevens et al., 2006, 2008; Mason et al., 2009)

Table DR1. OSL ages of Luochuan 2012

Lab No.	Sites	Depth (cm)	Water (%)	K(%)	U(ppm)	Th(ppm)	Does rate (Gy/Ka)	DE(Gy)	Aliquots	Age(a)
NJU163	LC	0	5±2	1.99±0.04	2.60±0.11	13.00±0.38	4.03±0.16	2.59±0.10	38	0.64±0.04
NJU144	LC	10	5±2	2.02±0.04	2.62±0.10	12.8±0.36	4.05±0.16	2.50±0.11	23	0.62±0.04
NJU145	LC	20	5±2	1.93±0.04	2.81±0.10	13.1±0.38	4.04±0.17	1.90±0.03	24	0.47±0.02
NJU146	LC	30	5±2	2.04±0.04	2.56±0.11	13.2±0.38	4.08±0.17	2.98±0.11	24	0.73±0.04
NJU147	LC	40	5±2	2.05±0.04	2.59±0.10	13.50±0.35	4.12±0.17	4.96±0.14	24	1.20±0.06
NJU148	LC	50	5±2	2.10±0.04	2.59±0.11	13.40±0.38	4.16±0.17	9.03±0.38	20	2.17±0.13
NJU149	LC	60	5±2	2.13±0.04	2.39±0.10	13.10±0.37	4.09±0.16	15.08±0.61	24	3.68±0.21
NJU150	LC	70	5±2	2.06±0.04	2.55±0.10	13.00±0.36	4.06±0.16	16.86±0.48	24	4.15±0.20
NJU151	LC	80	5±2	2.02±0.04	2.40±0.10	12.20±0.35	3.91±0.16	17.39±0.73	18	4.45±0.26
NJU152	LC	90	5±2	1.76±0.03	2.42±0.10	11.8±0.33	3.63±0.15	23.10±0.92	20	6.37±0.36
NJU153	LC	100	5±2	1.94±0.03	2.44±0.10	12.30±0.34	3.85±0.15	24.08±1.55	15	6.27±0.47
NJU154	LC	110	5±2	1.81±0.03	2.37±0.10	11.40±0.35	3.62±0.15	28.54±1.13	20	7.88±0.45
NJU155	LC	120	5±2	1.85±0.03	2.24±0.09	11.00±0.34	3.58±0.14	24.72±0.62	32	6.90±0.32
NJU156	LC	130	5±2	1.85±0.03	2.40±0.10	11.20±0.35	3.65±0.15	23.48±0.47	19	6.44±0.29
NJU157	LC	140	5±2	1.78±0.04	2.36±0.10	11.50±0.36	3.59±0.15	31.22±1.04	19	8.69±0.46
NJU158	LC	150	5±2	1.84±0.03	2.49±0.10	12.10±0.35	3.74±0.15	24.35±2.64	21	6.51±0.75
NJU159	LC	160	5±2	1.81±0.03	2.30±0.09	11.2±0.34	3.57±0.14	29.87±1.40	17	8.37±0.52
NJU160	LC	170	5±2	1.85±0.03	2.12±0.10	11.60±0.36	3.59±0.14	38.11±1.19	15	10.62±0.54
NJU135	LC	180	5±2	1.91±0.04	2.26±0.09	11.40±0.33	3.67±0.15	40.99±1.68	17	11.18±0.64
NJU132	LC	190	5±2	1.85±0.03	2.29±0.10	11.90±0.36	3.66±0.15	34.46±2.93	17	9.41±0.89
NJU134	LC	200	5±2	1.89±0.04	2.49±0.11	10.80±0.32	3.66±0.15	62.79±2.34	14	17.15±0.94
NJU139	LC	210	5±2	1.86±0.04	2.42±0.10	11.30±0.34	3.65±0.15	70.38±2.35	28	19.26±1.02
NJU136	LC	220	5±2	1.88±0.04	2.20±0.10	12.30±0.36	3.69±0.15	64.81±3.05	13	17.55±1.09
NJU133	LC	230	5±2	1.97±0.04	2.61±0.10	12.30±0.36	3.90±0.16	70.21±2.79	9	18.00±1.03
NJU138	LC	240	5±2	1.90±0.04	2.45±0.10	11.70±0.34	3.73±0.15	72.70±2.98	18	19.49±1.13
NJU141	LC	250	5±2	2.00±0.04	2.50±0.10	11.80±0.34	3.85±0.16	75.87±2.42	13	19.72±1.01
NJU143	LC	260	5±2	1.90±0.04	2.32±0.10	11.30±0.34	3.65±0.15	67.97±4.24	12	18.61±1.38
NJU161	LC	270	5±2	1.88±0.03	2.34±0.10	11.80±0.37	3.68±0.15	85.08±2.63	20	23.11±1.18
NJU162	LC	280	5±2	1.88±0.03	2.30±0.10	10.90±0.36	3.59±0.14	92.44±1.88	12	25.77±1.15
NJU142	LC	290	5±2	1.94±0.04	2.58±0.10	12.50±0.35	3.87±0.16	78.16±4.26	15	20.19±1.38
NJU140	LC	300	5±2	2.03±0.03	2.57±0.10	11.90±0.35	3.90±0.16	91.93±3.07	12	23.59±1.22

Table DR2. OSL ages of Yulin 2012

Lab No.	Sites	Depth (cm)	Water (%)	K(%)	U(ppm)	Th(ppm)	Does rate (Gy/Ka)	DE(Gy)	Aliquots	Age(a)
NJU221	ZBT	120	2.25	2.13±0.04	2.09±0.09	10.6±0.32	7.92±0.28	3.34±0.18	20	2.38±0.16
NJU222	ZBT	300	1.29	2.26±0.04	1.00±0.06	4.67±0.18	20.18±1.16	2.82±0.13	16	7.15±0.53
NJU223	ZBT	500	0.28	2.33±0.04	0.39±0.04	2.11±0.12	35.89±2.82	2.58±0.11	16	13.91±1.23
NJU224	ZBT	700	0.36	2.28±0.04	0.83±0.05	3.10±0.14	48.50±5.30	2.67±0.12	16	18.14±2.14
NJU225	ZBT	1500	3.57	1.89±0.04	2.16±0.09	10.5±0.30	133.00±6.32	2.94±0.17	16	45.30±3.44

2. Equivalent dose determination

Equivalent doses (D_e) were determined by using the single-aliquot regenerative-dose (SAR) protocol (Murray and Wintle, 2000). In order to select an appropriate preheat temperature, preheat plateau tests were conducted for typical samples (LC270cm and LC0cm from LC section, ZBT1.2m from YL section). As shown in Fig. DR2, a plateau was formed independently temperatures from 180 °C to 260 °C when using the preheat temperatures of 180 °C to 280 °C with a step of 20 °C.

The suitability of the SAR procedure for De determination was checked by 'dose recovery test' (Murray and Wintle, 2003). It examines the combined function of all the conditions of the protocol, such as preheat temperature, size of test dose. The dose recovery test was performed on two samples (LC270cm for LC section, ZBT1.2m for YL section). After complete bleaching with blue light at room temperature, the eight to twelve aliquots were irradiated with laboratory beta doses (given dose) which approximately equal to their natural dose (De) for each sample; they were then measured by the SAR protocol with a preheat of 220 °C for 10 s for LC samples and 240 °C for 10 s for YL samples. Given laboratory doses (79 Gy for LC270cm and 6.48 Gy for ZBT1.2m) could be reproduced with ratios of 0.96 ± 0.01and 1.00 ± 0.03. Therefore, a preheat temperature of 220 °C (for 10 s) can be selected for LC section and 240°C (for 10 s) for YL section De determination.

Examples of OSL decay curve and growth curve for sample LC0cm and ZBT1.2m were shown in Fig. DR3. The OSL signal decreases very quickly during the first second stimulation (Fig. DR3), which indicates the OSL signal at LC and YL is 'fast component' dominant. Recuperation was in all cases negligible (<3%) and for most of the aliquots the recycling ratios fall into the range of 0.9-1.1. A few discs with a recycling ratio falling outside this range were rejected in the final De calculation.

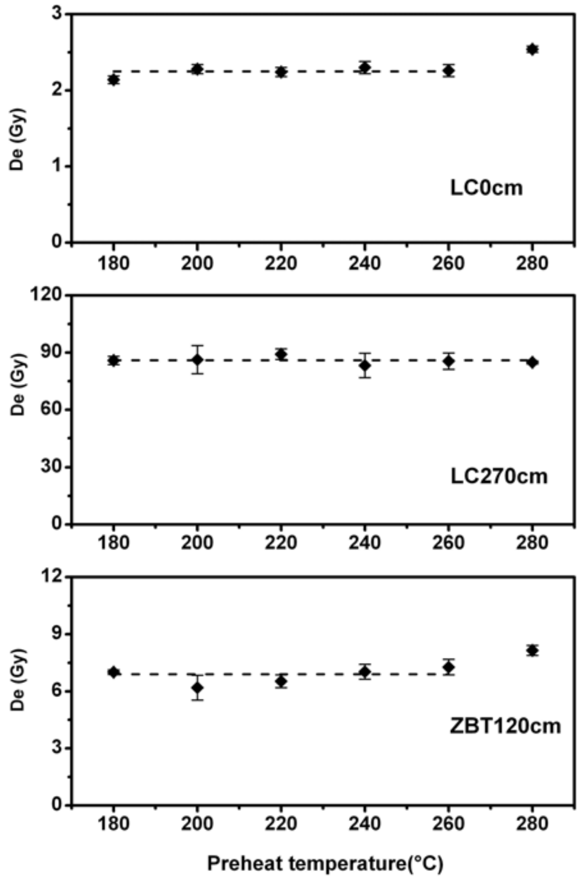

Figure DR2. Plot of equivalent dose against preheat temperature. It shows the dependence of equivalent dose on preheat temperature from 180 to 260°C，each point represents average of results from three aliquots.

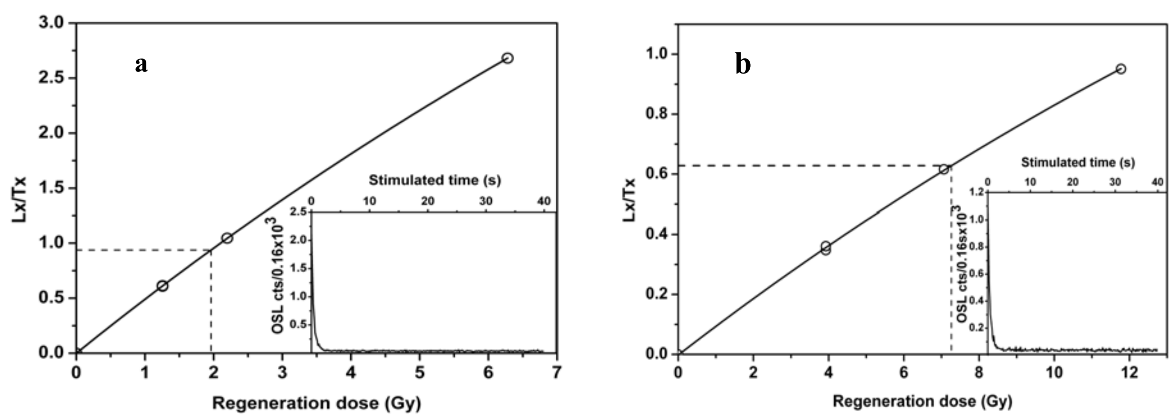

DATA REPOSITORY ITEM DR2

Paleoclimatic implication of carbon stable isotopic composition ($\delta^{13}C$), magnetic susceptibility (MS) and total organic matter (TOC) and the statistic analyses

Organic carbon stable isotopic composition ($\delta^{13}C$) of loess in the Loess Plateau is a measure of ratio of soil carbon input from C4 and C3 plants (Lin and Liu, 1992; Zhang et al., 2003; Liu et al., 2055a, b; Vidic and Montañez, 2004; Zhang et al., 2013). The C4 and C3 plants have different photosynthetic pathways that result in different responses to temperature and moisture. Many modern investigations show that vegetation composition in the Loess Plateau is controlled by the EASM precipitation (Lv et al., 2002; Wang et al., 2003; Rao et al., 2010; Lu et al. 2012; Chen et al., 2013) increasing monsoon precipitation favors C4 grasses that cause the $\delta^{13}C$ value to be more positive. Therefore, the $\delta^{13}C$ value can be used as proxy indicator of the monsoon strength. We measured the carbon stable isotopic composition of the total organic matter of the YL loess section and the compound-specific values of n-alkanes of samples of LC and XY sections; the YL $\delta^{13}C$ data are reported for the first time in this paper, while those from the LC and XY profiles have previously been reported (Zhang et al., 2003); but all three are analyzed here for the first time using new independent OSL age constraints. The measurement errors are less than ±0.3 ‰, much smaller than the variability in which is greater than ± 4‰; thus, the data are precise enough to interpret variations as the result of changes in monsoon precipitation. For technical details of the $\delta^{13}C$ measurements, see references (Lu et al., 2012).

MS of the loess in Chinese Loess Plateau has for a long-time been used as a proxy index of the EASM precipitation (Zhou et al., 1990; An et al., 1991; Maher et al., 1994; Maher and Hu, 2006), in that more humid and warmer climate was associated the strengthened EASM precipitation can enhance formation of magnetic minerals such as magnetite and hematite, and therefore increase the MS. Some studies have used MS to quantitatively reconstruct monsoon precipitation (Maher et al., 1994), although more investigations needed. We measured MS at all three sections using Bartington Magnetic Susceptibility MS-2 Meter. The MS of YL and LC are reported for the first time in this paper; our current measurement results are similar to the published data at Luochuan (Lu et al., 1999).

TOC content varies with plant biomass in natural vegetation of the semi-arid monsoon-dominated Chinese Loess Plateau. When the plant biomass was greater, more TOC was accumulated in the soil; on the other hand, a decrease of the TOC is induced by less plant biomass. Because the plant biomass is significantly associated with the EASM monsoon precipitation (Jia and Lin, 1993; Liu et al., 2005a; Lu et al., 2005, 2012), therefore, TOC can be used as a proxy index of monsoon precipitation. We measured TOC contents of the YL and LC sections, which covary with the MS (Fig. 2).

Table DR3. The proxy indicators data of published in this paper

Yulin data				Luochuan data	
Age (ka)	MS (SI)	TOC(%)	δ13C(‰)	Age(ka)	MS (SI)
0.00	32.67	0.26	-21.84	0.64	131.17
0.16	29.50	0.19	-20.86	0.67	143.00
0.32	28.33	0.20	-20.61	0.70	125.50
0.47	32.50	0.20	-20.73	0.73	132.00
0.63	32.67	0.21	-20.82	1.20	149.33
0.79	33.33	0.19	-20.54	2.17	167.33
0.95	39.67	0.32	-20.69	3.68	159.17
1.24	40.17	0.24	-20.81	4.15	139.67
1.52	35.33	0.22	-21.14	4.45	125.67
1.81	29.00	0.20	-20.94	6.37	96.33
2.10	39.50	0.19	-20.74	6.66	90.67
2.38	57.33	0.28	-20.73	6.94	85.83
2.67	69.67	0.44	-21.21	7.23	72.67
2.97	125.17	0.95	-22.01	7.51	96.00
3.27	135.83	0.82	-21.83	7.80	68.67
(Continued)					
3.58	134.67	1.29	-21.79	8.08	71.67
3.88	150.33	1.76	-21.75	8.37	67.50
4.18	143.17	1.03	-21.76	10.62	48.83
4.48	138.17	1.07	-21.40	12.80	51.50
4.78	150.50	1.14	-21.17	14.97	55.33
5.09	162.33	1.20	-21.59	17.15	47.50
5.39	168.67	1.28	-21.68	17.66	45.83
5.69	154.83	1.15	-21.57	18.18	53.50
5.99	125.33	0.85	-21.47	18.69	54.17
6.29	101.83	0.80	-21.15	19.21	60.67
6.59	80.33	0.59	-21.05	19.72	70.17
6.90	70.83	0.65	-21.26	20.49	66.67
7.20	57.83	0.58	-21.25	21.27	76.00
7.50	74.17	0.55	-21.05	22.04	80.83
7.64	42.17	0.29	-21.03	22.82	82.83

7.78	34.83	0.20	-20.77	23.59	83.83
7.91	31.67	0.15	-21.15		
8.05	28.33	0.15	-21.68		
8.19	23.00	0.13	-22.27		
8.33	19.83	0.11	-22.61		
8.46	21.67	0.11	-22.57		
8.60	20.50	0.08	-23.39		
8.74	20.33	0.08	-23.45		
9.17	17.50	0.06	-23.26		
9.61	15.00	0.06	-23.49		
10.04	11.83	0.03	-23.83		
10.47	9.17	0.03	-24.82		
10.91	9.33	0.03	-24.03		
11.34	4.17	0.02	-24.99		
11.77	5.33	0.03	-24.65		
12.20	9.17	0.02	-24.75		
12.64	9.00	0.02	-24.50		
13.07	24.33	0.03	-24.77		
13.50	22.67	0.03	-23.56		
13.94	15.83	0.03	-24.04		
14.37	4.67	0.03	-24.38		
14.80	3.33	0.02	-24.58		
15.24	5.33	0.02	-25.08		
15.67	5.83	0.02	-25.35		
16.10	5.33	0.02	-24.43		
16.53	4.33	0.02	-24.87		
16.97	5.83	0.02	-24.40		
(Continued)					
17.40	8.67	0.02	-24.44		
17.83	7.67	0.02	-25.19		
18.27	8.33	0.02	-24.10		
18.70	7.00	0.02	-25.17		
19.13	3.33	0.02	-25.06		
19.56	7.83	0.02	-25.14		
19.99	6.33	0.03	-24.74		
20.42	6.33	0.02	-23.93		
20.85	10.67	0.02	-24.43		
21.28	3.33	0.03	-24.12		
21.71	9.67	0.02	-25.20		
22.14	4.83	0.02	-25.59		

In order to statistically analyze correlation coefficients between the proxy indicators of EASM precipitation and insolation, CO_2, ice volume, Greenland temperature and Antarctic temperature, we normalized all the data series as variability between -1 and +1 (Fig. DR4, DR5 and DR6). The correlation between the EASM monsoon proxy time series (combined normalized $\delta^{13}C$ time series from YL, LC and XY as shown by Fig. DR4) with the CO_2 has a coefficient of 0.734 at the 99% level (2-tailed student-T test) (Table 1), may suggest a linkage of the two factors.

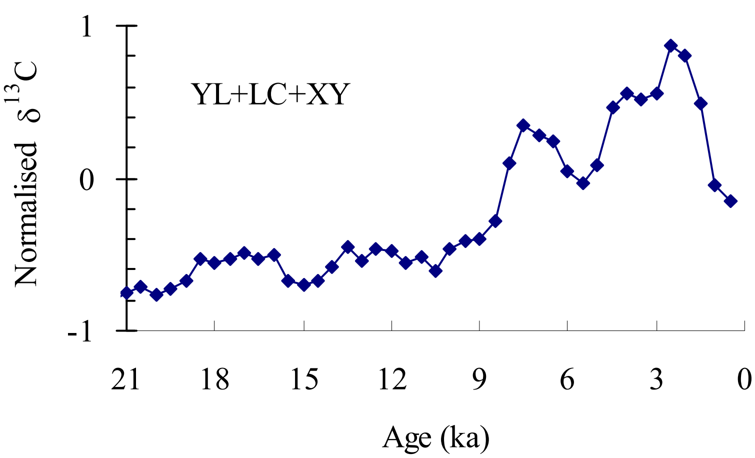

Figure DR4. Combined normalized $\delta^{13}C$ of Yulin, Luochuan and Xunyi loess-paleosol sequences

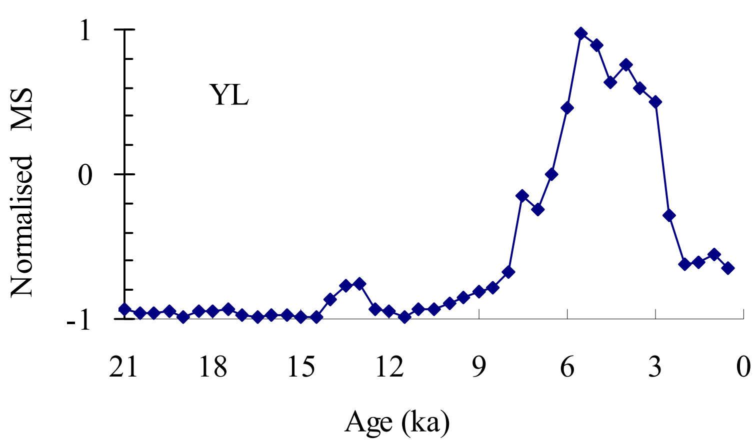

Figure DR5. Normalized MS of Yulin loess-paleosol sequence

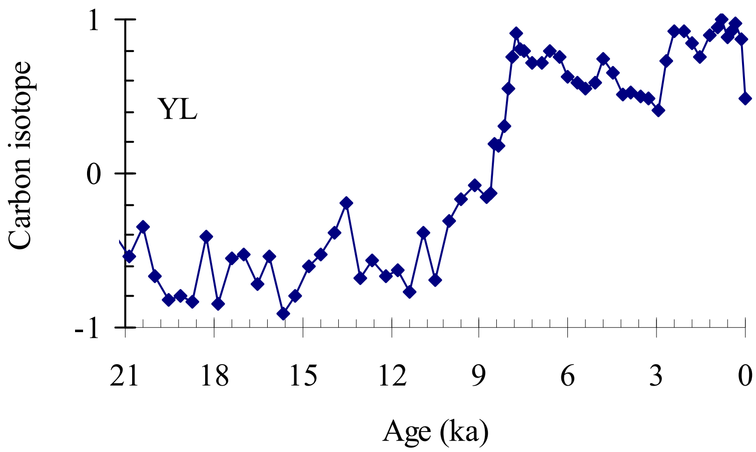

Figure DR6. Normalized $\delta^{13}C$ of Yulin loess-paleosol sequence

DATA REPOSITORY ITEM DR3

Paleoclimatic modeling: Testing CO_2 modulated the EASM precipitation

We used the TraCE-21000 modeling to test interpretation of this study. The TraCE-21000 is carried out in a synchronously coupled ocean–atmosphere–sea ice–land surface climate model without flux adjustment - the National Center for Atmospheric Research (NCAR) Community Climate System Model version 3 (CCSM3, Collins et al., 2006), in the version of T31_gx3v5 resolution (Yeager et al., 2003). The atmospheric model is the CAM3 with horizontal resolution of about 3.75 ° × 3.75 ° and 26 vertical hybrid coordinate levels. The land model is CLM3 with same resolution as the atmosphere. The ocean model is the NCAR implementation of POP with vertical z-coordinate and 25 levels. The longitudinal resolution is 3.6 degree and the latitudinal resolution is variable, with finer resolution in the equator (~0.9 degrees). The sea ice model is the CSIM with same resolution as the ocean model.

The TraCE-21000 was initialized from an earlier LGM equilibrium simulation of CCSM3 (Otto-Bliesner et al., 2006), with adding dynamic vegetation to reduce the model drift in the deep ocean. The vegetation model is NCAR CLM2 with LPJ long term ecological dynamics. It is initialized in the coupled CCSM3 from the present but spun up at 22 ka for 2000 years to reach its LGM equilibrium. This transient simulation cover the period of 22 ~ 0 ka with realistic changes in boundary conditions and various forcings – the continental ice sheet and coastlines (Peltier, 2004), the orbital forcing (only its long-term variation, Berger, 1978), the green housing gas (GHG, including CO2, CH4 and N2O, Joos and spahni, 2008) forcing and the meltwater forcing (Liu et al., 2009, which referring to the reconstructed sea level changes in Peltier, 2004). The TraCE-21000 captures many major features of the deglacial climate evolution, for example, cooling during Heinrich event 1(H1), abrupt BA warming and cooling in Younger Dryas (YD) (Liu et al., 2009, 2012).

Annual precipitation values are lower (significant at the 95% level) in the LGM compared to the MH. The simulations show that reduced precipitation during the LGM and increase during the MH are associated with the CO_2 forced high-latitude temperature changes, which may push the ITCZ movements that determine variations of the EASM precipitation at orbital timescales since 21 ka.

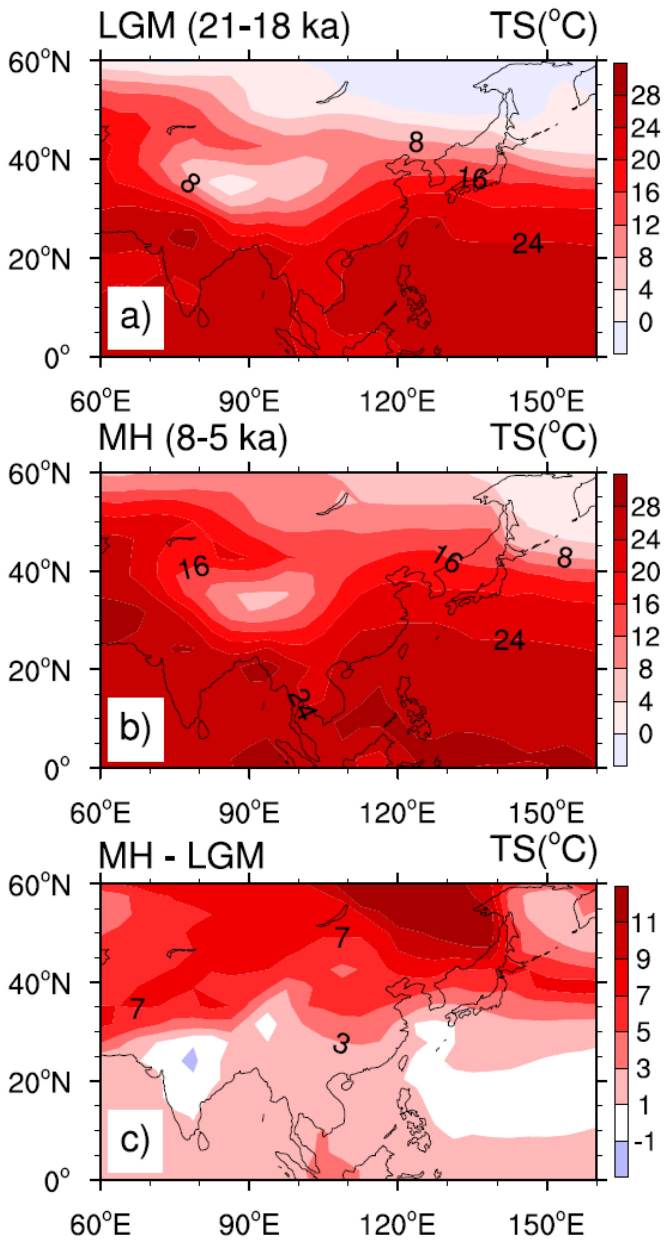

Figure DR7. Mean state of surface temperature (℃) at LGM (a, 21-18 ka) and MH (b, 8-5 ka), and their difference (c, MH minus LGM), in a transient simulation of Earth climate during the last 21 ka.

References Cited

Adamiec, G., Aitken, M.J., 1998, Dose rate conversion factors: update: Ancient Thermoluminescence, v. 16, p. 37-50.

Aitken, M. J. An introduction to optical dating. Oxford University Press, Oxford. 1998.

An, Z.S., Kukla, G.J., Porter, S.C., and Xiao, J.L., 1991, Evidence of monsoon variation on the Loess Plateau of central China during the last 130,000 years: Quaternary Research, v. 36, p. 29-36.

Berger, A., 1978, Long-term variations of daily insolation and Quaternary climatic changes: Journal of Atmosphere Science, v. 35, p. 2362–2367. doi: http://dx.doi.org /10.1175/ 1520-0469 (1978) 035<2362:LTVODI>2.0.CO;2

Bøtter-Jensen, L., Andersen, C.E., Duller, G.A. T., Murray, A.S., 2003, Developments in radiation, stimulation and observation facilities in luminescence measurements: Radiation Measurements, v. 37, p. 535-541.

Buylaert, J.P., Murray, A.S., Vandenberghe, D., Vriend, M.G. A., De Corte, F., Van den haute, P., 2007, Optical dating of Chinese loess using sand-sized quartz: establishing a time frame for late Pleistocene climate changes in the western part of the Chinese Loess Plateau: Quaternary Geochronology, v. 3, p. 99-113.

Chen, Y.Y., Lu, H.Y., Zhang, E.L, Zhou, Y.L., Wang, X.Y., Han, Z.Y., Xu, Z.W., 2013, The relationship between organic carbon isotopic composition of surface sediment and vegetation-climate in Otindag dunefield, northern China: Quaternary Sciences, v. 33, p. 351-359.

Collins, W.D., Rasch, P.J., Boville, B.A., Hack, J.J., McCaa, J.R., Williamson, D.L., Briegleb, B.P., Bitz, C.M., Lin, S.J., Zhang, M.H., 2006, The formulation and atmospheric simulation of the community atmosphere model version 3 (CAM3): Journal of Climate, v. 19, p. 2144–2161.

Duller, G.A.T., 2003, Distinguishing quartz and feldspar in single grain luminescence measurements: Radiation Measurements, v. 37, p. 161-165.

Grün, R., 2009, The “AGE” program for the calculation of luminescence age estimates: Ancient TL, v. 27, p. 45-46.

Jia, R.F. and Lin, B.H., 1993, Preliminary research on lipids in loess and paleosol of Duanjiapo section near Xi’an: Scientia Geographica Sinica, v. 13, p. 337-345.

Joos, F. and R. Spahni, 2008, Rates of change in natural and anthropogenic radiative forcing over the past 20 000 years: Proceedings of the National Academy of Sciences of the United States of America, v. 105, p. 1425–1430.

Lin, B.H. and Liu, R.M., 1992, The stable isotope evidence of the variance of the summer monsoon in the Loess Plateau from recent 800 ka: Chinese Science Bulletin, v. 18, p. 1691-1693.

Liu, W.G., Ning, Y.F., An, Z.S., Wu, Z.H., Lu, H.Y., Cao Y.N., 2005a, Carbon isotopic composition of modern soil and paleosol as a response to vegetation change on the China Loess Plateau: Science in Chin: Earth Sciences, v. 48, p. 93-99.

Liu, W.G., Huang, Y.S., An, Z.S., Clemens, S.C., Li, L., Prell, W.L., Ning, Y.F., 2005b, Summer monsoon intensity controls C4/C3 plant abundance during the last 35 ka in the Chinese Loess Plateau: carbon isotope evidence from bulk organic matter and individual leaf waxes: Palaeogeography Palaeoclimatology Palaeoecology, v. 220, p. 243–254.

Liu, Z., Carlson, A.E., He, F., Brady, E.C., Otto-Bliesner, B.L., Briegleb, B., Wehrenberg, M., Clark, P.U., Wu, S., Cheng, J., Noone, D. and Zhang, J. Younger Dryas cooling and the Greenland climate response to CO2: Proceedings of the National Academy of Sciences of the United States of America, v. 109, p. 11101-11104.

Liu, Z., Otto-Bliesner, B.L., He, F., Brady, E.C., Tomas, R., Clark, P.U., Carlson, A.E., Lynch-Stieglitz, J., Curry, W., Brook, E., Erickson, D., Jacob, R., Kutzbach, J., Cheng, J., 2009, Transient simulation of last Deglaciation with a new mechanism for Bølling-Allerød Warming: Science, v. 325, p. 310-314.

Lu, H.Y., Liu, X.D., Zhang, F.Q., An, Z.S. and Dodson, J., 1999, Astronomical calibration of loess-paleosol deposits at Luochuan, central Chinese Loess Plateau: Palaeogeography Palaeoclimatology Palaeoecology, v. 154, p. 237-246.

Lu, H.Y., Miao, X.D., Zhou, Y.L., Mason, J., Swinehart, J., Zhang, J.F., Zhou, L.P., and Yi, S.W. 2005, Late Quaternary aeolian activity in the Mu Us and Otindag dune fields (North China) and lagged response to insolation forcing: Geophysical Research Letters, v. 32, L21716, doi:10.1029/2005GL024560.

Lu, H.Y., Zhou, Y.L., Liu, W.G., and Mason, J., 2012, Organic stable carbon isotopic composition reveals late Quaternary vegetation changes in the dune fields of northern China: Quaternary Research, v. 77, p. 433–444.

Lv, D.R., Chen, Z.Z., Chen, J.Y., Wang, G.C., Ji, J.J., Chen, H., Liu, Z.L., Zhang, R.H., Qiao, J.S., Chen, Y.J., 2002, Composite study on Inner Mongolia semi-arid grassland soil-vegetation-atmosphere inter action (IMGRASS): Earth Science Frontiers, v. 9, p. 295-306.

Maher, B.A., Thompson, R., and Zhou, L.P., 1994, Spatial and temporal reconstructions of changes in the Asian palaeomonsoon: A new mineral magnetic approach. Earth and Planetary Science Letters, v. 125, p. 461-471.

Maher, B.A . Hu, M.Y., 2006, A high-resolution record of Holocene rainfall variations from the western Chinese Loess Plateau: Antiphase behaviour of the African/Indian and East Asian summer monsoons: Holocene, v. 16, p. 309-319.

Mason, J.A., Lu, H.Y., Zhou, Y.L., Miao, X.D., Swinehart, J.B., Liu, Z.Y., Goble, R.J. and Yi, S.W., 2009, Dune mobility and aridity at the desert margin of northern China at a time of peak monsoon strength: Geology, v. 37, p. 947–950.

Murray, A.S., Wintle, A.G.., 2000. Luminescence dating of quartz using an improved sinle-aliquot regenerative-dose protocol: Radiation Measurements, v. 32, p. 57-73.

Murray, A.S., Wintle, A.G., 2003, The single aliquot regenerative dose protocol: potential for improvements in reliability: Radiation Measurements, v. 37, p. 377-381.

Otto-Bliesner B., Brady E., Clauzet G., Thomas R., Levis S., & Z. Kothavala, 2006, Last glacial maximum and Holocene climate in CCSM3. Journal of Climate, v.

19, p. 2526–2544.
Peltier W. R., 2004, Global Glacial Isostasy and the Surface of the Ice-Age Earth: The ICE-5G (VM2) Model and GRACE: Annual Review of Earth and Planetary Science, v. 32, p. 111-149.
Rao, Z.G., Zhu, Z.Y., Jia, G.D., Chen, F.H., Barton, L., Zhang, J.W., Qiang, M.R., 2010, Relationship between climatic conditions and the relative abundance of modern C3 and C4 plants in three regions around the North Pacific: Chinese Science Bulletin, v. 55, p. 1931-1936.
Stevens T., Armitage, S.J., Lu, H.Y., and Thomas, D.S.G., 2006, Sedimentation and diagenesis of Chinese loess: Implications for the preservation of continuous high-resolution climate records: Geology, v. 34, p. 849-852.
Stevens, T., Lu, H.Y., Thomas, D.S.G. and Armitage, S.J., 2008, Optical dating of abrupt shifts in the Late Pleistocene East Asian monsoon: Geology, v. 36, p. 415-418.
Vidic, N.J., Montañez, I.P., 2004, Climatically driven glacial–interglacial variations in C3 and C4 plant proportions on the Chinese Loess Plateau: Geology**,** v. 32, 337–340.
Wang, G.A., Han, J.M., Liu, D.S., 2003, The carbon isotope composition of C3 herbaceous plants in loess area of northern China: Science in China: Earth Sciences, v. 46, p. 1069-1076.
Yeager, S.G., Shields, C.A., Large, W.G., and Hack J.J., 2006, The low-resolution CCSM3: Journal of Climate, v. 19, p. 2545-2566.
Zhang, Z.H., Zhao, M.X., Lu, H.Y., Faiia, A.M., 2003, Lower temperature as the main cause of C4 plant declines during the glacial periods on the Chinese Loess Plateau: Earth and Planetary Science Letters, v. 214, p. 467–481.
Zhang, X., Jia, X., Rao, Z.G., Dong, G. H., Zhang, D. J., 2013, C3/C4 variation since the last Glacial in the southeastern Longxi Loess Plateau and its comparison with other results: Quaternary Sciences, v. 33, p. 187-196.
Zhou, L.P., Oldfield, F., Wintle, A.G., Robinson S.G., Wang J. T., 1990, Partly pedogenic origin of magnetic variations in Chinese loess: Nature, v. 346, p. 737-739.